Fault identification in HVDC grids using a transient parametric model

Paul Verrax, Alberto Bertinato, Michel Kieffer, Bertrand Raison

Available online at www.sciencedirect.com

ScienceDirect

IFAC Papers Online CONFERENCE PAPER ARCHIVE

IFAC PapersOnLine 53-2 (2020) 13700–13706

Fault identification in HVDC grids using a transient parametric model

Paul Verrax [*,**] **Alberto Bertinato** [*] **Michel Kieffer** [**] **Bertrand Raison** [***]

[*] *Supergrid Institute, 23 rue Cyprian, 69 100 Villeurbanne (e-mail: paul.verrax@supergrid-institute.com).*

[**] *L2S, CNRS–CentraleSupelec–Univ Paris-Sud, Univ Paris-Saclay, 3 rue Joliot-Curie, 91192 Gif-sur-Yvette.*

[***] *Univ. Grenoble Alpes, CNRS, Grenoble INP*, G2Elab, 38000 Grenoble, France (* Institute of Engineering Univ. Grenoble Alpes).*

Abstract: This paper presents a novel single-ended fault identification algorithm for meshed High Voltage Direct Current grids. This algorithm can be used in the context of fully-selective fault-clearing strategies. Once a fault is suspected, using a parametric model describing the voltage and current evolution just after the fault occurrence, a maximum-likelihood estimate of the fault distance and impedance is evaluated. The presence of the fault is then confirmed depending on the size of the confidence region of the obtained estimate. The approach is evaluated on a simulated three-node meshed grid. The current and voltage need to be observed during less than 0.2 ms to get an accurate estimate of the fault characteristics and to identify consistently the faulty line.

Keywords: Power transmission, HVDC transmission lines, Parameter estimation, Fault identification, Maximum likelihood estimators

1. INTRODUCTION

Multi-Terminal high-voltage Direct Current (MTDC) grids will provide better interconnection over large distances between renewable energy sources and consumption area (Pierri et al., 2017). Among the barriers still to overcome for the development of High-Voltage Direct-Current (HVDC) meshed grids, the protection of the lines is seen as one of the most challenging (Van Hertem and Ghandhari, 2010).

The main tasks of a protection strategy include fault detection, faulty component identification, tripping of the breakers, and power restoring (WP4 PROMOTIoN, 2018). Selective fault clearing strategies consist in identifying the faulty line so as to trigger only the breakers of the faulty line. This minimizes the impact of the fault on the grid (Abedrabbo et al., 2017). Protection algorithms must detect and identify the fault fast enough, typically in less than a millisecond, to cope with the breaking capabilities of Direct Current Circuit Breaker (DCCB), which makes the use of communication between distant protection devices not suitable. Hence, a selective protection scheme requires single-ended algorithms ensuring selectivity, *i.e.*, able to discriminate between internal faults, occurring on the protected line and external faults, occurring elsewhere in the grid.

A faulty behavior is generally associated with high variation rates in both current and voltage. Various measurements-based methods using thresholds on voltage derivatives (Sneath and Rajapakse, 2016), or current derivatives (Azad et al., 2015), or both , have been proposed. They all benefit from costly inductances placed at the end of each line, between the relay and the busbar, see Figure 6. However, when considering overhead transmission lines such inductances could be omitted.

Model-based methods try to benefit from a more accurate description of the evolution of current and voltage when a fault appears on a line. In the context of AC transmission, (Banerjee et al., 2014) used a linearized power flow dynamics model of the system both before and after the fault. A quickest change detection approach is then applied to detect as fast as possible a change in the probability distribution of the phase angles. Still in AC, but considering the transient behavior, multiple traveling wave arrival times are considered in (Guzman-Casillas et al., 2018) to spot the reflection patterns between the observation point and the fault. Several wave arrival times (about a dozen) need to be acquired, which limits the speed of the method. A multiple behavioral model-based approach has been developed in (Ali Al Hage et al., 2015). Universal line models are derived for a finite set of possible fault cases. These models are combined in a bank of Kalman filters used to perform the fault identification. Measurements from the relay are then compared to the predictions obtained from the filters. The best predicting filter provides an estimate of the fault characteristics. This technique requires considering many

⋆ This work was carried out at the SuperGrid Institute, an institute for the energetic transition (ITE). It is supported by the French government under the frame of "*Investissements d'avenir*" program with grant reference number ANE-ITE-002-01.

10.1016/j.ifacol.2020.12.873

filters so as to be able to identify faults with a large variety of characteristics.

Model-based algorithms are hence considered for fault detection and identification. Nevertheless, finding a good trade-off between quick detection and identification and accurate (therefore complex) estimation of the fault characteristics is still challenging.

This paper introduces a novel single-ended protection algorithm able to detect and identify faults occurring on transmission lines. Each relay embeds a parametric model of the evolution of the current and voltage in case of a fault, depending on a set of physical fault parameters. When a fault is suspected, an iterative maximum-likelihood (ML) estimate of the fault parameters is evaluated from the data available at the relay. The estimated fault parameters and their confidence intervals are exploited to determine whether or not one has to consider that a fault actually occurred on the protected line. Section 2 describes the problem formulation and the proposed approach. The modeling of the fault behavior is detailed in Section 3. Simulation results are presented in Section 4.

2. PROBLEM FORMULATION AND PROPOSED APPROACH

An MTDC grid is described by a graph $\mathcal{G} = (\mathcal{V}, \mathcal{E})$, where $\mathcal{E}$ is a set of edges, representing the lines connecting pairs of nodes represented by the vertices in $\mathcal{V}$. The nodes may consist of converter stations or other equipments such as sensors, relays, *etc.* Consider some vertex $q \in \mathcal{V}$ connected to n_q lines. Within the node represented by q, each line is assumed to be monitored by some fault identification device (FID) in charge of determining whether the line under protection is faulty. Due to detection and identification delay constraints, the FID hosted by different stations do not have the possibility to exchange information.

Consider a fault occurring at some time instant t_f on a given line $e = (q, q') \in \mathcal{E}$ of length $d_{qq'}$ connecting stations q and q'. The distances between the fault and the stations q and q' are $d_{\mathrm{f},q}$ and $d_{\mathrm{f},q'} = d_{qq'} - d_{\mathrm{f},q}$. The fault is assumed to be characterized by its pole-to-ground or pole-to-pole impedance Z_f depending on the type of fault, considered constant during the time interval of interest in the order of a millisecond. The vector of parameters describing a fault is thus $\mathbf{p} = (e, d_{\mathrm{f},q}, Z_\mathrm{f}, t_\mathrm{f})^\mathrm{T}$. During the parameter estimation process the line e is fixed. Furthermore $d_{\mathrm{f},q}$ and t_f are linked through the detection time of the first traveling wave at station q, $t_{\mathrm{d},q} = t_\mathrm{f} + \frac{d_{\mathrm{f},q}}{c_\mathrm{w}}$, which can be measured. c_w is the propagation speed of the traveling waves, determined by the line parameters (Allan Greenwood, 1991). Thus the vector of the fault parameters can be reduced to $\mathbf{p} = (d_{\mathrm{f},q}, Z_\mathrm{f})^\mathrm{T}$.

Assume that the FID of vertex q monitoring line e acquires at a frequency f voltage and current measurements $(v_{q,e}(t), i_{q,e}(t))$ at the end of e connected to q. Using, *e.g.*, an under-voltage criterion (Kong et al., 2014), the FID is able to determine whether the grid behaves normally or not.

Once an abnormal behavior has been detected, the FID has to determine whether or not the fault occurred in the monitored line. The proposed approach, see Figure 1, considers a parametric model of the evolution of voltage and current at node q when a fault occurs. An ML estimate of the vector of fault parameters $\mathbf{p}$ is evaluated from the voltage and current measurements $(v_{q,e}(t), i_{q,e}(t))$. The model depends on the characteristics of the grid (supposed known) and on $\mathbf{p}$. For a given value of $\mathbf{p}$, the output at time t of the model is denoted as $\left(v^\mathrm{m}_{q,e}(t,\mathbf{p}), i^\mathrm{m}_{q,e}(t,\mathbf{p})\right)$. The model combines a knowledge-based model derived from physical principles and a behavioral model used to account for additional effects such as soil resistivity.

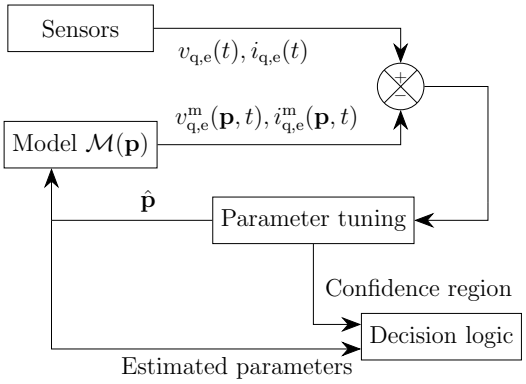

Fig. 1. Overview of the proposed fault identification approach.

Consider that the fault actually occurred on the line e with parameters $\mathbf{p}^*$. Assuming that the voltage and current measurements noise sample are zero-mean Gaussian and uncorrelated, the ML estimate $\widehat{\mathbf{p}}$ of $\mathbf{p}^*$ leads to the minimization of the following cost function by the FID (Walter and Pronzato, 1997)

$$c^{(n)}(\mathbf{p}) = \mathbf{f}^{(n)}(\mathbf{p})^T \left(\widetilde{\Sigma}^{(n)}\right)^{-1} \mathbf{f}^{(n)}(\mathbf{p}), \tag{1}$$

where

$$\mathbf{f}^{(n)}(\mathbf{p}) = \Big[\left(v(t_1) - v^\mathrm{m}(\mathbf{p}, t_1)\right), \ldots, \left(v(t_n) - v^\mathrm{m}(\mathbf{p}, t_n)\right) \left(i(t_1) - i^\mathrm{m}(\mathbf{p}, t_1)\right), \ldots, \left(i(t_n) - i^\mathrm{m}(\mathbf{p}, t_n)\right)\Big]^T, \tag{2}$$

and $\widetilde{\Sigma}^{(n)}$ is a diagonal matrix containing the measurement noise variances for the voltage and current sensors. The number of measurement points n is increased each time Δn new measurements are available.

For each $\widehat{\mathbf{p}}$, an approximate confidence region $\mathcal{R}^{(\alpha)}(\widehat{\mathbf{p}})$ is evaluated. To determine whether the estimate is consistent with the hypothesis that the monitored line is faulty, two tests are considered. First, a *validity* test determines whether $\widehat{\mathbf{p}}$ is included in some domain of interest. Second, an *accuracy* test determines whether the area of the 95% confidence region of the estimated parameters $\mathcal{R}^{(\alpha)}(\widehat{\mathbf{p}})$ goes under some threshold tr_{95}. This confidence region is computed based on the Fisher information matrix (Walter and Pronzato, 1997). If both tests are satisfied, the fault is deemed to affect line e. When it is unable to conclude, the FID waits for the availability of Δn additional measurements to update $\widehat{\mathbf{p}}$ and $\mathcal{R}^{(\alpha)}(\widehat{\mathbf{p}})$. Thus the estimation algorithm uses all the available measurements at each time by increasing regularly the size of the cost function (2).

Once enough measurements [1] have been made available without allowing the FID to conclude, the fault is deemed to be located elsewhere in the grid, or to be non-existent.

3. DC FAULT ANALYTIC MODELING

This section presents the model introduced to describe the evolution of the current and voltage measured at the end of a line affected by a fault. The considered model combines a knowledge based model described in Section 3.1, and a behavioral model described in Section 3.2, see Figure 2.

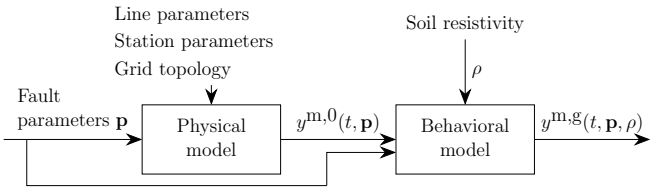

Fig. 2. Two-layer combined physical and behavioral model

3.1 Physical model

The transient behavior of current and voltage measured at a given point of a line e connecting stations q and q' can be modeled using traveling waves (Sohn et al., 2016). The telegraph equations (Allan Greenwood, 1991) allow one to represent the propagation and attenuation of the voltage and current waves as they travel along the line. The reflections and transmissions of those waves may be described by a Bewley lattice diagram, see Figure 3 for the case of a three station network, as presented in Figure 6, connecting stations q, q', and q''. The station q'' is represented on both sides of the diagram.

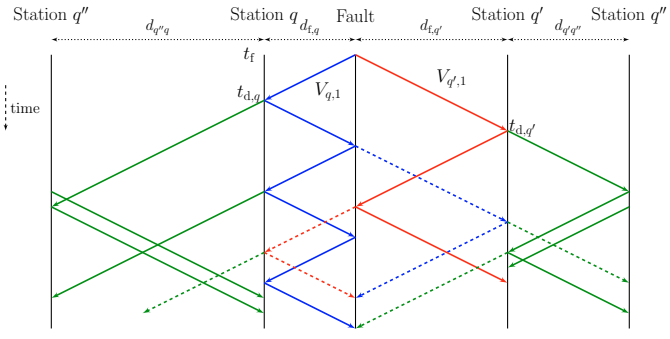

Fig. 3. Example of a Bewley lattice diagram.

The evolution of the current and voltage at station q has to account for several traveling waves (see Figure 3):

– due to the first incident wave from the fault to station q; this wave is reflected by station q and by the fault (plain blue lines),

– due to the first incident wave from the fault to station q', reflected by station q', and transmitted by the fault (dashed red lines),

– due to the transmission of the incident waves to other lines of the grid or which have been transmitted several times by the fault (dashed blue and green lines).

Expressions for these different waves can be explicitly derived in the Laplace domain, assuming that $\mathbf{p}$ is known. A resistive fault is considered and an RLC equivalent is used for the converter stations (Leterme and Van Hertem, 2014). Furthermore, a loss-less approximation proved to have sufficient accuracy when modeling the propagation of the waves along the line. This, however, neglects the effects of the soil resistivity. Considering these assumptions, it is possible to analytically compute the inverse Laplace transform of the expressions for the different waves. One then obtains time-domain expressions, not detailed here due to lack of space, which depend explicitly on $\mathbf{p}$ as well as the physical parameters of the grid.

3.2 Modeling the impact of the soil resistivity

To simplify analysis, one represents the soil resistivity by a known constant parameter ρ along the return path of the line e. To account for soil resistivity effects, the physical model of Section 3.1 is supplemented with a behavioral model, to get a *combined* model, Figure 2.

Consider the output $y^{\mathrm{m},0}(\mathbf{p},t) = (v^{\mathrm{m},0}(t,\mathbf{p})^T, i^{\mathrm{m},0}(t,\mathbf{p})^T)^T$ of the model in Section 3.1, representing the voltage and current at a given point of the monitored line e. Preliminary simulations have shown that the soil resistivity impacts the model output $y^{\mathrm{m},0}(\mathbf{p},t)$ as a low-pass filter, see also Figure 4. Consequently, we choose to describe the output $y^{\mathrm{m,g}} = (v^{\mathrm{m,g}}(t,\mathbf{p})^T, i^{\mathrm{m,g}}(t,\mathbf{p})^T)^T$ of the model accounting for the effects of the soil resistivity as

$$y^{\mathrm{m,g}}(t_k,\mathbf{p},\rho) = \underbrace{\frac{z^{-n_{\mathrm{d}}}(b_0+\cdots+b_{n_{\mathrm{b}}}z^{-n_{\mathrm{b}}})}{1-a_1z^{-1}-\cdots-a_{n_{\mathrm{a}}}z^{-n_{\mathrm{a}}}}}_{=G(z^{-1},\boldsymbol{\theta})} y^{\mathrm{m},0}(t_k,\mathbf{p}), \tag{3}$$

where n_{d} models the input-output delay and $\boldsymbol{\theta} = (a_1,\ldots,a_{n_{\mathrm{a}}},b_0,\ldots,b_{n_{\mathrm{b}}},n_{\mathrm{d}})^T$. The same filter is used for the voltage and for the current. An offline estimation of n_{d} and of the coefficients a_i and b_i may then be performed considering the measurements $y(t) = \left(v(t)^T, i(t)^T\right)^T$ for a vector of known fault parameters $\mathbf{p}$ using, *e.g.*, the Electro-Magnetic Transient (EMT) software EMTP-RV (Mahseredjian et al., 2007), taken a K time instants $t_1,\ldots,t_K$ after the occurrence of a fault. For a given value of $\mathbf{p}$ and of ρ, a least-squares (Ljung, 1987) estimate $\widehat{\boldsymbol{\theta}}$ of $\boldsymbol{\theta}$ is computed, *i.e.*,

$$\widehat{\boldsymbol{\theta}} = \arg\min_{\theta} \sum_{k=1}^{K} \|y(t_k) - y^{\mathrm{m,g}}(t_k,\mathbf{p},\rho,\boldsymbol{\theta})\|_2^2. \tag{4}$$

First traveling wave Figure 4 represents an example of the evolutions of voltage and current at a station for the first traveling wave generated by a fault. The considered grid for the simulations is detailed in Section 4. The estimation of the parameters of the soil resistivity filters has been performed considering only the first traveling

[1] The first traveling wave contains enough information to obtain a consistent estimate of the fault parameters. The largest time interval between the fault inception of the first wave and the arrival time of a second wave is used as maximum measurement window, *i.e.*, $\tau_{\max} = d_{qq'}/c_w \sim 1$ ms for a 300 km long line.

wave for both current and voltage. One observes that the outputs of the combined model accounting for the soil resistivity ($\rho > 0$) are much closer to the outputs provided by EMTP-RV than the outputs of the physical model neglecting the soil resistivity ($\rho = 0$). For the considered behavioral model $G\left(z^{-1}\right)$, considering $n_\mathrm{a} = 1$, $n_\mathrm{b} = 0$ provides the best compromise between accuracy and evaluation complexity.

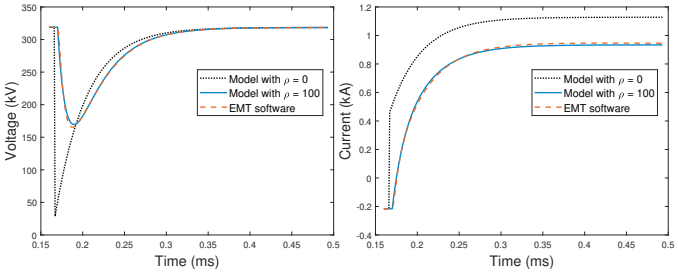

Fig. 4. Comparison of the voltage (left) and current (right) transient models, neglecting or accounting for the soil resistivity with the output of an EMT simulation software; the simulated fault is located 50 km away from the station and has a resistance of 20 Ω; the soil resistivity is $\rho = 100\,\Omega\mathrm{m}$.

The coefficients of the transfer function G that models the effect of soil resistivity clearly depend on the value of ρ. Additional simulations have also evidenced the impact of the components of the fault parameter vector $\mathbf{p}$, among which the distance to the fault d_f is the most important. In order to get a behavioral model of the impact of the soil resistivity that is valid whatever the fault location, one explicitly accounts for d_f in the parameters a_i and b_i of the model. Figure 5 describes the evolution of the coefficients a_1 and b_0 as estimated for different values of the fault distance d_f considering $\rho = 100\,\Omega\mathrm{m}$. Second order polynomial models in $1/d_\mathrm{f}$ are considered to model the evolution of a_1 and b_0 with d_f, while n_d is taken as the floor of a second order polynomial in d_f, $n_\mathrm{d}^\mathrm{m}\left(d_\mathrm{f}\right)$. The parameters of those polynomials have again been adjusted by least squares estimation. The evolution of a_1^m, b_0^m, and n_d^m with d_f is also provided in Figure 5, showing an excellent match with the estimated values of a_1, b_0, and n_d.

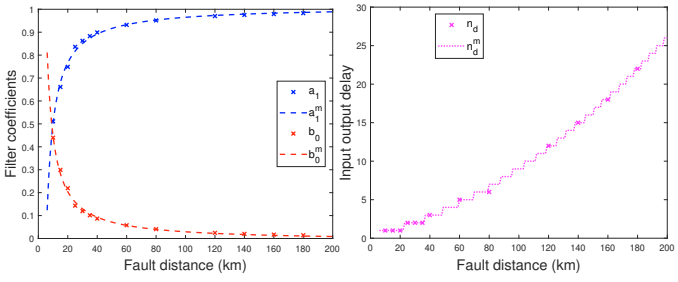

Fig. 5. Evolution of the estimated parameters a_1, b_0 (left) and n_d (right) as a function of d_f (crosses), compared to their modeled evolution $a_1^\mathrm{m}\left(d_\mathrm{f}\right)$ and $b_0^\mathrm{m}\left(d_\mathrm{f}\right)$ (left) and n_d^m (right) (dashed and dotted lines)

Other traveling waves To account for the effect of soil resistivity for other traveling waves, one assumes that the distance d in the parameters $a_1^\mathrm{m}\left(d\right)$ and $b_0^\mathrm{m}\left(d\right)$ of the model (3) has to represent the sum of the traveled distance. For instance, the first traveling wave, once it has been reflected by the station and at the fault location, when it reaches again the station, has traveled three times the fault distance (see Figure 3). The combined model output $y^{\mathrm{m,g}}$ is obtained by filtering the physical model output $y^{\mathrm{m},0}$ with a filter G which parameters are $a_1^\mathrm{m}\left(3d_\mathrm{f}\right)$, $b_0^\mathrm{m}\left(3d_\mathrm{f}\right)$, and $n_\mathrm{d}\left(3d_\mathrm{f}\right)$.

4. SIMULATION RESULTS AND DISCUSSION

Measurements in case of faults are provided by EMTP-RV and the FID is implemented in Matlab. The test grid is first introduced and an illustrative example of the algorithm is detailed in Section 4.1. More extensive simulations are then carried out in Section 4.2.

4.1 Illustrative example

Consider a meshed grid with identical single-conductor overhead lines and 3 MMC stations, see Figure 6. This reduced grid can be seen as an elementary brick for larger meshed grids since. Indeed, the presence of additional stations further than 300 km from the fault would not influence the transient during the first ms. FID in relays R_{ij} and R_{ji} monitor line L_{ij} of length d_{ij}, $1 \leqslant i < j \leqslant 3$. The current and voltage sensors used in the EMT simulations have an accuracy class of 1 %, a bandwidth of 300 kHz, a sampling frequency of 1 MHz, and a resolution of 16 bits. Conversion stations have a rated power of 1 GW. The additional parameters have been taken from (WP4 PROMOTIoN, 2018). The estimation algorithm is initialized at $\mathbf{p}_\mathrm{init} = (R_\mathrm{init}, d_\mathrm{init}) = (1\,\Omega, 6\text{ km})$. The number of data points added after each iteration is fixed at $\Delta n = 10$. The maximum measurement window that can be used to determine whether the line is faulty is set to d/c_w for a relay monitoring a line of length d where waves propagate at a speed c_w.

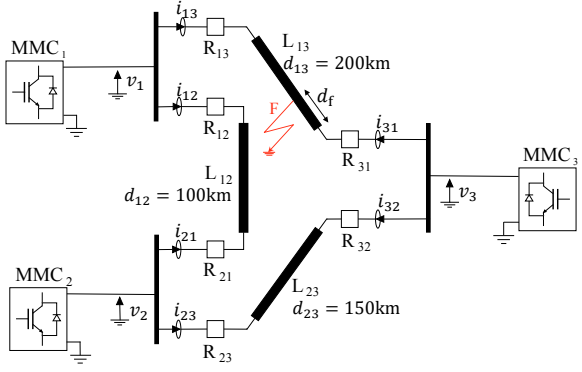

Fig. 6. Test grid where an asymmetrical monopole (WP4 PROMOTIoN, 2018) with single conductor configuration and earth return is considered

One considers a pole-to-ground fault occurring at $t_\mathrm{f} = 0$ in line L_{13} of the grid in Figure 6 at a distance $d_\mathrm{f}^* = 80$ km from station 3 with an impedance of $R_\mathrm{f}^* = 40\ \Omega$. Once an abnormal behavior is detected at relay R_{31}, the identification algorithm is started. Its behavior can be analyzed by plotting the contour of the cost function to be minimized at each iteration as well as the trajectory of the estimate $(d_\mathrm{f}, R_\mathrm{f})$ of the fault parameter vector, see Figure 7. The

95% confidence ellipse of the estimated parameter vector is also displayed at iterations 5 and 9. After each iteration, when new data points are taken into account, the argument of the minimum gets closer to (d_f^*, R_f^*) and the cost contours concentrate around (d_f^*, R_f^*). The estimate $(\widehat{d}_f, \widehat{R}_f)$ also gets closer to (d_f^*, R_f^*) and the size of the confidence ellipsoid reduces. The estimation algorithm stops and correctly identifies the fault on the line after 9 iterations, requiring only measurements obtained in a time window of 96 μs. The estimated parameters are $\widehat{d}_f = 68$ km and $\widehat{R}_f = 55\,\Omega$ when the algorithm stops.

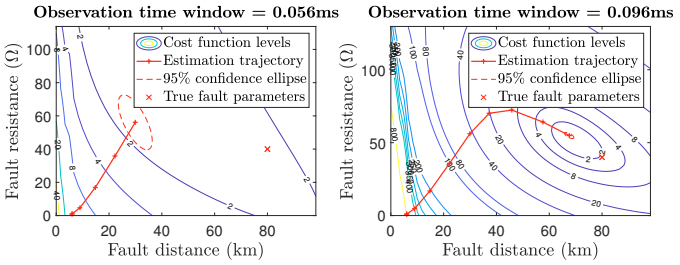

Fig. 7. Fault at $d_f^* = 80$ km from station 3 with an impedance of $R_f^* = 40\,\Omega$: evolution of the contour plot of the cost function and estimated parameters at iterations 5 and 9.

The voltage and current measurements simulated by the EMT software and the output the combined model of Section 3.2 for $\widehat{d}_f = 60$ km and $\widehat{R}_f = 54\,\Omega$ are represented in Figure 8. One sees that the observation of the first wave is enough for an accurate fault identification.

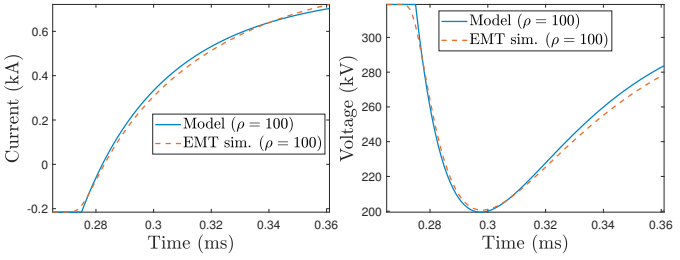

Fig. 8. Simulated current (left) and voltage (right) measurements compared to the combined model outputs for $\widehat{d}_f = 55$ km and $\widehat{R}_f = 68\,\Omega$.

There is no guarantee that the optimization problem defined in (1) is convex. Different initial points may hence lead to different local optima. This is studied by comparing the evolution of the estimated parameters when using different initial points. Five different initializations have been considered, $\mathbf{p}_{\text{init}}(\Omega, \text{km}) = \{(1, 6), (1, d_{13}), (100, 0.5d_{13}), (200, 6), (200, d_{13})\}$, where $d_{13} = 200$ km. The results on Figure 9 show all the different initialization lead to identical estimates in about 100 μs, corresponding to tens iterations. Thus, the resulting choice of $\mathbf{p}_{\text{init}} = (1\,\Omega, 6\,\text{km})$ only speeds up the convergence when faults are close with low impedance. This is beneficial as such faults are the most severe and require particular fast identification. In practice, multiple parallel initialization could be considered to increase the robustness of the algorithm.

The behavior of the identification algorithm at the other relays is analyzed by plotting the evolution of the confidence region area at the 6 relays, Figure 10. The threshold for the accuracy test is set to $tr_{95} = 10$. Even if the fault is rapidly identified at relays R_{31} and R_{13}, the evolution of the accuracy criterion is plotted until the maximum measurement window is reached to facilitate comparison with the evolution of the criterion at the other relays. Since the fault is close to station 3, it is first detected at relays R_{31} and R_{32}. The accuracy test is satisfied at relay R_{31} after 12 iterations and the fault is identified in line L_{13}, as shown previously. At relay R_{32} the area of the confidence region never goes below the threshold, indicating that the fault is not in line L_{23}. At $t = 0.5$ ms the fault is detected at the other end of L_{13}. At relay R_{13}, the fault is again correctly identified after few iterations whereas at relay R_{12}, the accuracy test is never satisfied. The fault finally reaches the third station at $t = 0.8$ ms where, as expected, neither R_{21} nor R_{23} identify the fault to be on their respective protected line. This illustrates that the method is able to identify internal faults using very few measurements while rejecting faults occurring on neighboring lines. More extensive simulations regarding the selectivity of the proposed method with respect to external faults can be found in (Verrax et al., 2020). Moreover, Figure 10 shows there is some freedom in the selection of the threshold used. A threshold 10 times larger or smaller would not have changed the identification results at the different relays but only the identification speed at relays R_{13} and R_{31}.

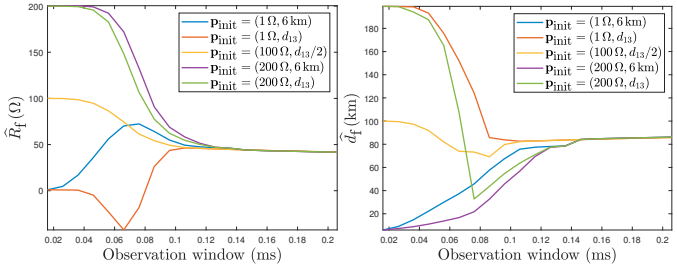

Fig. 9. Evolution of the estimated parameters for different initial points on a typical observation window of 200 μs.

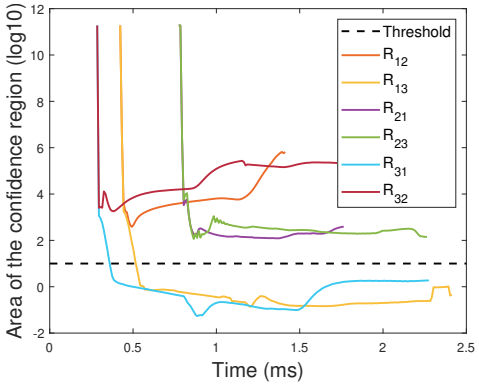

Fig. 10. Evolution of the confidence region area at the 6 relays

4.2 Extensive simulations

To test the behavior of the algorithm on a broader range of fault cases, more extensive simulations were carried out considering 54 different single fault scenarios with parameters (R_f, d_f) affecting the line between Stations 1 and 3,

with the resistance $R_f \in \{0, 15, 35, 60, 90, 160\}\,\Omega$ and the distance $d_f \in \{5, 15, 35, 90, 110, 120, 150, 160, 180\}$ km. The fault distance d_f is taken with respect to station 3 and the performance of the algorithm embedded within the relay R_{31} is studied. We compare the ability of the algorithm to correctly identify faults as internal to the protected line in two different configurations. First when the model is only composed of the physical part that neglects the soil resistivity (see Section 3.1) and second the model is extended with the behavioral part (see Section 3.2) that represents more faithfully the effects of the soil resistivity. In Figure 11, the light blue area corresponds to faults correctly identified using either the physical or extended model. The dark green area corresponds to fault cases for which the algorithm fails to identify the fault when using only the physical model but succeeds when considering the extended model. Thus, the extended model extend the domain of applicability of the algorithm to high impedance faults as well as faults occurring farther from the relay, hence covering the total length of the protected line.

The amount of data required to perform the fault identification (considering only cases for which the algorithm successfully identifies the fault) using the two different models is compared in Figure 12. One can see that taking into account the soil resistivity effects in the model largely decreases the amount of data required for fault identification. This is notably because performing consistent fault parameters estimation without taking into account the soil resistivity effects require the observation of more waves (at least two). In particular the objective of being able to identify at each step faults in less than 1 ms can only be met when using the extended model.

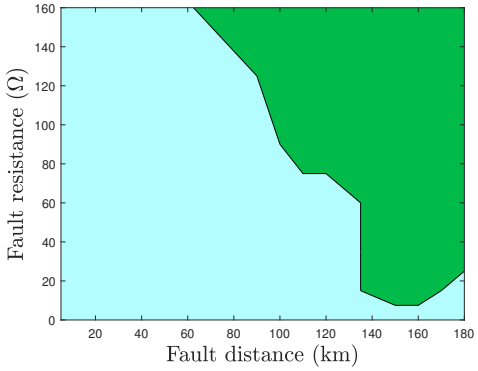

Fig. 11. Region of fault parameters that leads to a correct identification depending on the model used. The green area corresponds to the additional fault cases detected using the extended model whereas the light blue area corresponds to the fault cases identified using either model.

5. CONCLUSION

This paper presents a novel single-ended algorithm for fault identification for meshed HVDC grids. A parametric model consisting of a physical part and a behavioral part is used to describe the voltage and current evolution just after the occurrence of a fault. Then, a maximum-likelihood estimate of the fault parameters is performed and updated each time new measurements are available. The confidence region associated to the parameter estimate is used to decide if the fault affects the protected line or if more measurements are needed. The approach is evaluated on a simulated three-node meshed grid. On the vast majority of fault cases the current and voltage must be observed during less than 0.2 ms to get an accurate estimate of the fault characteristics and to identify consistently the faulty line. To further improve the robustness and the precision of the proposed approach, one can run several estimation algorithms with different initialization within the same relay and rely on a voting system among the provided estimates.

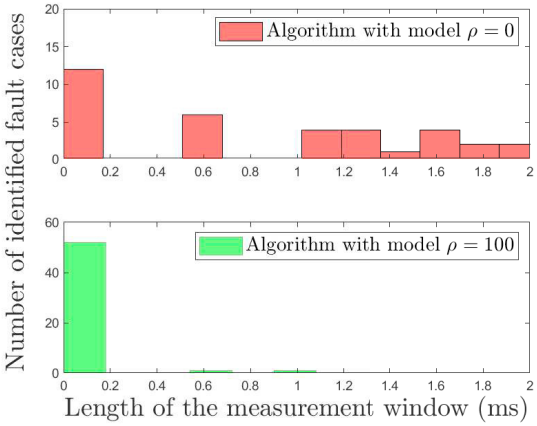

Fig. 12. Comparison of the length of the observed measurement window required for successful identification depending on the model used ($\rho = 0$ in red and $\rho = 100$ in green). Here the maximum measurement window has been set to 3 ms to facilitate the comparison between the two model performances.

REFERENCES

Abedrabbo, M., Wang, M., Tielens, P., Dejene, F.Z., Leterme, W., Beerten, J., and Van Hertem, D. (2017). Impact of DC grid contingencies on AC system stability. In *Proc. 13th IET International Conference on AC and DC Power Transmission (ACDC 2017)*, CP709, 1–7.

Ali Al Hage, A., Piepenbreier, B., Buchstaller, D., and Engel, M. (2015). A multiple model approach to fault detection and localization in multi-terminal HVDC systems. In *Proc. IECON 41st Annual Conference of the IEEE Industrial Electronics Society*, 1–5.

Allan Greenwood (1991). *Electrical Transients in Power Systems*. John Wiley & Sons, 2nd ed. edition.

Azad, S.P., Leterme, W., and Van Hertem, D. (2015). A DC grid primary protection algorithm based on current measurements. In *Proc. 17th European Conference on Power Electronics and Applications, EPE-ECCE Europe*, 1–10. Geneva.

Banerjee, T., Chen, Y.C., and Dom, A.D. (2014). Power system line outage detection and identification - A quickest change detection approach. *Proc. IEEE International Conference on Acoustics, Speech and Signal Processing - Proceedings (ICASSP)*, 3474–3478.

Guzman-Casillas, A., Kasztenny, B., Tong, Y., and Mynam, M.V. (2018). Accurate single-end fault locating using traveling-wave reflection information. In *Proc. Developments In Power System Protection*, 1–6. Belfast.

Kong, F., Hao, Z., Zhang, S., and Zhang, B. (2014). Development of a novel protection device for bipolar HVDC transmission lines. *IEEE Transactions on Power Delivery*, 29(5), 2270–2278.

Leterme, W. and Van Hertem, D. (2014). Reduced Modular Multilevel Converter Model to Evaluate Fault Transients in DC Grids. In *Proc. 12th IET International Conference on Developments in Power System Protection (DPSP)*.

Ljung, L. (1987). *System Identification - Theory for the User*. Prentice-Hall, Englewood Cliffs, NJ.

Mahseredjian, J., Dennetière, S., Dubé, L., Khodabakhchian, B., and Gérin-Lajoie, L. (2007). On a new approach for the simulation of transients in power systems. *Electric Power Systems Research*, 77(11), 1514–1520.

Pierri, E., Binder, O., Hemdan, N.G., and Kurrat, M. (2017). Challenges and opportunities for a European HVDC grid. *Renewable and Sustainable Energy Reviews*, 70, 427–456.

Sneath, J. and Rajapakse, A.D. (2016). Fault Detection and Interruption in an Earthed HVDC Grid Using ROCOV and Hybrid DC Breakers. *IEEE Transactions on Power Delivery*, 31(3), 971–981.

Sohn, S.H., Cho, G.J., and Kim, C.H. (2016). Development of Power System Transient Analysis Program based on Traveling Wave Theory using MATLAB. In *Proc. IFAC Workshop on Control of Transmission and Distribution Smart Grids*, volume 49, 230–234. Elsevier B.V., Prague.

Van Hertem, D. and Ghandhari, M. (2010). Multi-terminal VSC HVDC for the European supergrid: Obstacles. *Renewable and Sustainable Energy Reviews*, 14(9), 3156–3163.

Verrax, P., Bertinato, A., Kieffer, M., and Raison, B. (2020). Transient-based fault identification algorithm using parametric models for meshed HVDC grids. *Electric Power Systems Research*, 185(April). doi:10.1016/j.epsr.2020.106387. URL `https://doi.org/10.1016/j.epsr.2020.106387`.

Walter, E. and Pronzato, L. (1997). *Identification of parametric models from experimental data*. Springer-Verlag London.

WP4 PROMOTIoN (2018). Report on the broad comparison of protection philosophies for the identified grid topologies. Technical report.